ASSESSMENT OF THE LIFTING LINE APPROXIMATION FOR WIND TURBINE BLADE MODELLING

Tonio Sant
University of Malta
tonio.sant@um.edu.mt

Vanessa del Campo
UPC (ETSEIAT)
vanessa.del.campo@upc.edu

Daniel Micallef
TUDelft (DUWIND)
D.Micallef@tudelft.nl

Carlos Simão Ferreira
TUDelft (DUWIND)
C.J.SimaoFerreira@tudelft.nl

Abstract

Lifting line vortex approaches have been widely used to predict rotor flow fields. Nonetheless, there could be some deficiencies in the flow field close to the blade due to the assumption that blade vorticity is concentrated on a line. The present study thoroughly assessed the errors arising from this approximation by prescribing the bound circulation as a boundary condition on the flow, using an inverse lifting-line free-wake vortex approach. The prescribed bound circulation was calculated front two independent sources using (1) experimental results from PIV and (2) data generated from a 3D panel free-wake vortex approach, where the blade geometry is fully modelled. The flow field around the blades from the inverse lifting line vortex model was then compared with those directly produced by SPIV and the 3D panel model.

Keywords: Lifting line, free-wake vortex model, SPIV, panel method, blade design, angle of attack, bound circulation, aerodynamics.

1. Introduction

Understanding the aerodynamics of a wind turbine is fundamental to predict the rotor dynamic loads, energy yield, noise generation and wake evolution. A thorough review of the state of the art and the progress in this field can be found in [1,2,3,4]. Since the character of the Navier-Stokes equations is such that their Direct Numerical Simulation (DNS) is unfeasible for practical purposes, other numerical approaches have been developed in order to obtain the flow field around and behind the rotor.

On the one hand, the Blade Element and Momentum Theory (BEMT) approach, in which the rotor is modelled as an actuator disc, is still the most common method for engineering design applications. The method is simple, however, it lacks the physics necessary to capture certain rotor aerodynamic phenomena with a sufficient level of detail. On the other hand, solving the Navier-Stokes equations with simplifying assumptions such as Reynolds Averaging (RANS) is more physically comprehensive, but its implementation is still too computationally expensive.

Vortex wake methods offer a compromise between the above mentioned methods. In these approaches, the flow is assumed to be incompressible and inviscid while vorticity formed at the blades is convected into the wake as trailing and shed vorticity with a local velocity equal to the sum of the free stream velocity and that induced by all vorticity sources (from the wake and blades). The circulation in the wake is modelled by a series of vortex filaments that can take the form of lines [5, 6] or particles [7, 8]. Circulation around the blades is modelled with a lifting line or a lifting surface.

Panel methods apply the same approach for modelling the wake, but the blade geometry is taken into account more accurately. Viscous effects can be included with a boundary layer

model. Consequently, panel methods are computationally more demanding than a lifting line method. Therefore, the lifting line model is convenient in routine engineering computations given that it allows for direct input of aerofoil lift and drag data.

The present study is aimed at assessing the capability of the lifting line approach integrated with a free-wake vortex model for simulating the flow distribution around rotating wind turbine blades. The discrepancies between the flow field predictions in the central parts of the blade, where the flow is mostly 2D, and the outer part of the blades, where 3D flow phenomena become more dominant, will also be discussed.

This paper is organised as follows: The methodology and the rotor geometry used will be described first. Secondly, the experimental techniques (Stereo Particle Image Velocimetry) and the numerical models (Panel Vortex and Inverse Lifting Line with Free Vortex Wake) utilized will be introduced. Finally, the results obtained will be discussed and the main conclusions from this study will be presented.

2. Methodology

The study analyzed the axial (V_a) and tangential (V_t) flow velocity components in the close vicinity of the wind turbine blades, with the rotor operating at a fixed tip speed ratio λ = 7. Such conditions yielded low angles of attack over the entire blade, hence the flow around the blades could be assumed to be fully attached. The flow field at six different planes located at *r/R* equal to 0.4, 0.55, 0.7, 0.82, 0.9 and 0.96 was considered, with each plane aligned with local blade cross section. The following independent experimental data and numerical codes were used to obtain V_a and V_t across at each of these six planes:

a) Stereo Particle Image Velocimetry experimental measurements (PIV).

b) 3D Panel Vortex model code (PC).

c) Inverse Lifting-Line Free-Wake Vortex code (LN) with a prescribed bound circulation distribution $\Gamma_B(r)$ derived from the Panel code (PC) computations.

d) Inverse Lifting-Line Free-Wake Vortex code (LN), with a prescribed bound circulation distribution $\Gamma_B(r)$ estimated directly from the SPIV measurements.

Figure 1 depicts schematically the flow of work conducted for this investigation.

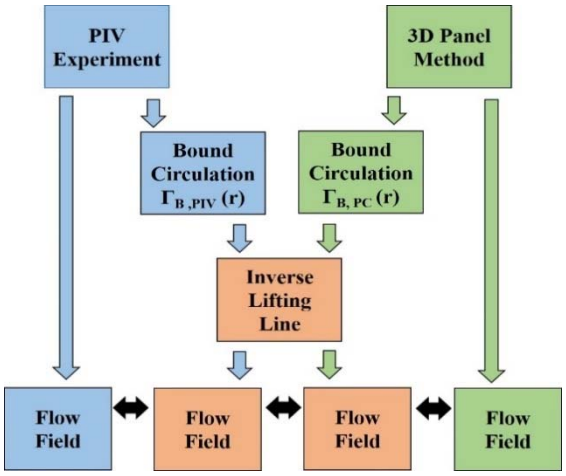

Figure 1: *Flow of Work*

3. Rotor Geometry

The tested HAWT model consisted of 2 blades and had a total radius of *R* = 1 m. It was operated by an electrical engine that turned it at a constant angular velocity of 400 rpm. The blade sections had the geometric profile of a DU-96-W180 aerofoil. The blade was not pitched but it was tapered and twisted, as can be seen in Figure 2.

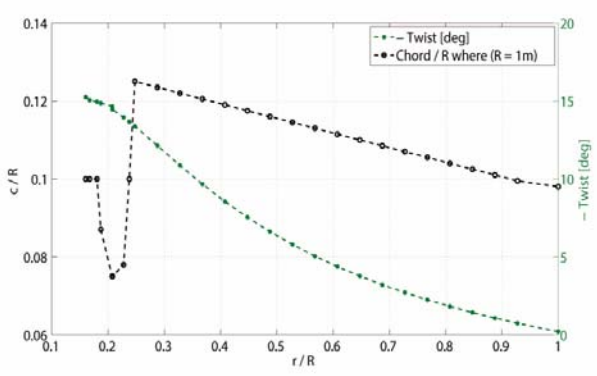

Figure 2*: Twist and Chord distribution*

4. SPIV and Experimental Apparatus

The experimental campaign presented herein was performed at the Open Jet Facility (OJF) at TUDelft. The closed circuit wind tunnel has an octagonal jet exit equivalent to a 3m diameter and the size of the test section is 6 x 6.5 x 13.5 m^3. The flow velocity was fixed to 6 m/s.

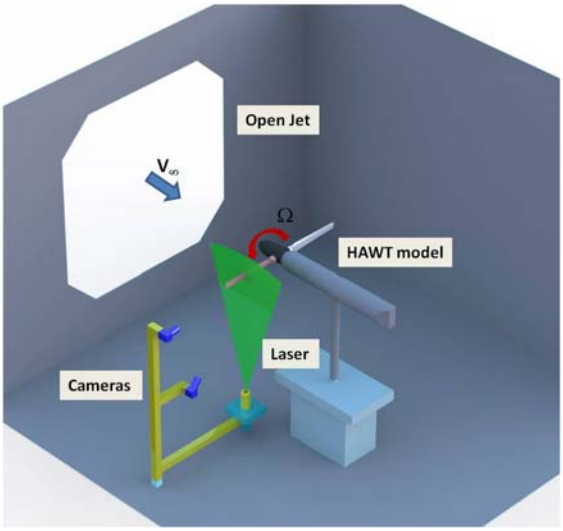

Figure 3: *SPIV Experimental Set Up*

The HAWT model was tested in axial conditions, as shown in Figure 3. One hundred SPIV images were obtained for each phase-locked velocity plane. Two cameras and the laser were mounted in a computerized traverse system. Table 1 presents main PIV imaging and acquisition parameters.

SPIV Parameters

Laser Type	NdYAG (300mJ)
Seeding	Diethylene Glycol and Water
Camera Resolution	4830x 3230px^2
Field of View	230 x210mm^2
Spatial Resolution	1.8mm
InterrogationWindow	32x32(50% overlap)

Table 1: *PIV Imaging and Acquisition Parameters*

The domain at each plane was rectangular (23 by 21cm), positioned to encompass the entire blade section and with the longer sides aligned parallel to the rotorplane. Mean bound vorticity was calculated from each PIV plane considered, using 10 different rectangular paths surrounding the blade. Further details on the experiment can be found in [9, 10].

5. Panel Free Wake Vortex Model

The panel method model used is a 3D model that assumes potential flow and can solve multi-body, unsteady problems. The blades are modeled with 3D surface panels of sources and doublets with a constant distribution. The non-entry requirement on the airfoil surface is implemented by imposing a Dirichlet boundary condition on the potential function. As the blades rotate, a wake of free convecting doublets is released from the trailing edge. By imposing the Kutta condition the vorticity at the trailing edge is set to zero. Therefore, the near wake doublet strength is given by the difference in doublet strengths between upper and lower surfaces of the airfoil. Viscous effects are accounted for through the use of vortex core and vortex core growth models proposed by [11, 12]. The influence of filament stretching on the core size of the individual filaments is also modeled. Finally, the far wake is modeled with a mesh of vortex rings. The model contains methods to realistically treat blade-wake interactions and vortex stretching and contraction. More information about the panel code (PC) can be found in [10, 13, 14, 15].

6. Inverse Lifting Line Free Wake Vortex Model

The inverse lifting line free-wake code (LN) was developed by [16]. The code generates an inflow distribution across any defined plane from a known bound circulation distribution prescribed by the user at the blades. Each blade is modeled using lifting line piecewise elements, with their width decreasing gradually towards the blade tip and root in accordance with a cosine distribution. The near wake is modeled using a vortex sheet per blade, each consisting of a mesh of filaments to account for both trailing and shed vorticity shed by the rotating blades. Viscous effects in the near wake are accounted for through the use of vortex core

models at each filament, accounting for core growth and the influence of filament stretching. In the present study the core models of [11, 12] were implemented in the same way as for the panel code described in section 5. A far wake model is also included though this is limited to a single prescribed helix per blade to approximate a fully rolled up tip vortex.

7. Results and Discussion

A 2D grid linear interpolation was applied within the six radial planes to all numerical predictions to estimate the flow velocities at the grid nodes for which the PIV measurements were available. In order to assess quantitatively the capability of lifting-line free-wake vortex method in modelling the flow around rotating wind turbine blades, the following relative errors (see Table 2, where *U* is the free stream velocity) were computed at each grid node:

$\varepsilon_{1,a} = \frac{V_{a,PC} - V_{a,PIV}}{U}$	$\varepsilon_{1,t} = \frac{V_{t,PC} - V_{t,PIV}}{U}$
$\varepsilon_{2,a} = \frac{V_{a,LN} - V_{a,PC}}{U}$	$\varepsilon_{2,t} = \frac{V_{t,LN} - V_{t,PC}}{U}$
$\varepsilon_{3,a} = \frac{V_{a,LN} - V_{a,PIV}}{U}$	$\varepsilon_{3,t} = \frac{V_{t,LN} - V_{t,PIV}}{U}$
(1a,b,c)	(2a,b,c)

Table 2: *Velocity Relative Errors*

It should be pointed out that the error computations were performed for the situation in which the bound circulation, hence the blade lift, distribution of the lifting line model is equal to that of the panel code and measurements, respectively (see Figure 1). The error computations were not conducted in the close vicinity of the blade's surface given the technical constraints of the adopted PIV measurement technique.

Figure 4 plots the radial distributions of the two bound circulation distributions that were obtained independently from the panel code (PC) and PIV measurements. Differences between the two distributions are small and are mainly due to errors in the PIV measurements and limitations of the panel vortex model code in modelling the viscous flow phenomena at the blade surfaces and in the wake.

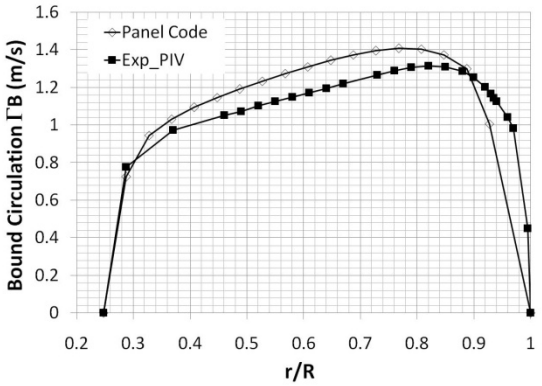

Figure 4: *Bound circulation distributions obtained independently for the TUDelft rotor using the panel code and PIV measurements*

Figure 5 presents the contour plots for the errors $\varepsilon_{2,a}$ and $\varepsilon_{3,a}$ in the axial flow velocities. Figures (a)-(c) highlight the differences between the lifting-line free wake model (LN) predictions at *r/R* equal to 0.4, 0.7 and 0.96 and those from the panel code (PC). Figures (d)-(e) show the differences between the lifting-line (LN) predictions and the PIV measurements. The relatively error is largest close to the blades, decreasing to lower than 10% further away from the aerofoil. Comparing Figures 5 (a)-(c) and (d)-(f), one can note a relatively good agreement between the spatial distribution of the relative error based on the panel code prediction $\varepsilon_{2,a}$ and the PIV measurements $\varepsilon_{3,a}$.

It is possible to clearly identify from Figure 5 the regions around the blades at which the lifting line free wake model is capable of modelling the axial component of the flow reliably. These regions are mainly located further away from the blades, although there exist confined areas in the proximity of the blades where the lifting line model predictions are still in good agreement with those of the panel code and the PIV measurements. The latter areas are located at the leading and trailing edges of the blade sections and at the mid-chord upper and lower blade surfaces

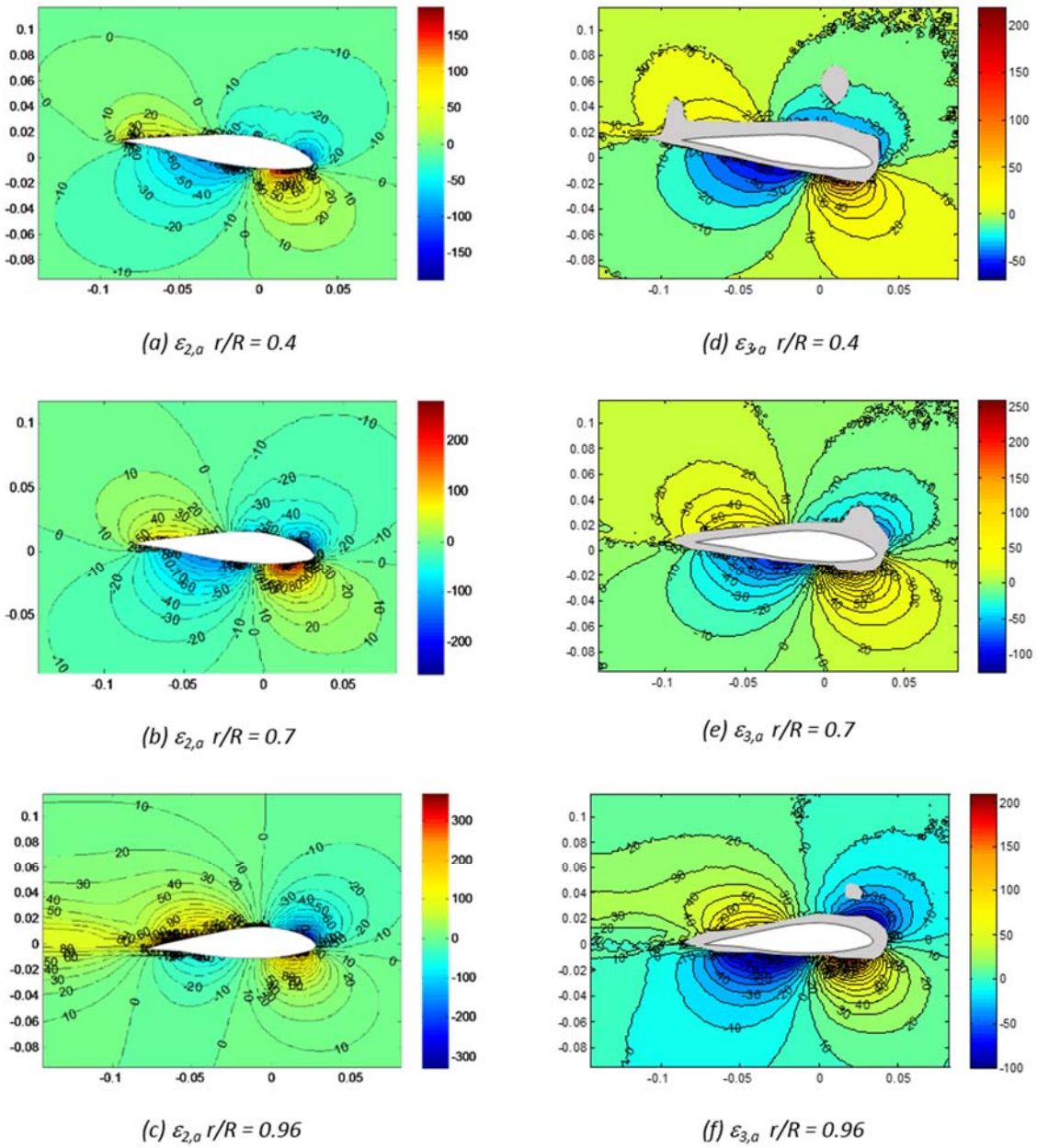

Figure 5: *Contour plots showing distributions for percentage errors $\varepsilon_{2,a}$((a)-(c)) and $\varepsilon_{3,a}$ ((d)-(f)) around the blades. The x and y coordinates for the flow domain are shown in metres.*

As may be noted from Figures 5 (c) and (f), the region across which errors $\varepsilon_{2,a}$and $\varepsilon_{3,a}$are high at *r/R*=0.96 is larger than for the inboard sections. This is a consequence of the complex 3D flow field induced by the blade tip geometry and the formation of the strong tip vortex in the near wake. The lifting-line representation of the blades is less capable than panel methods in capturing such three-dimensional effects. Yet, there still exist areas at the outer most regions within the domain at 0.96*R* at which the lifting line model prediction errors $\varepsilon_{2,a}$ and $\varepsilon_{3,a}$are < 10%.

Figure 6 illustrates the contour plots for the lifting line model errors in tangential velocities.

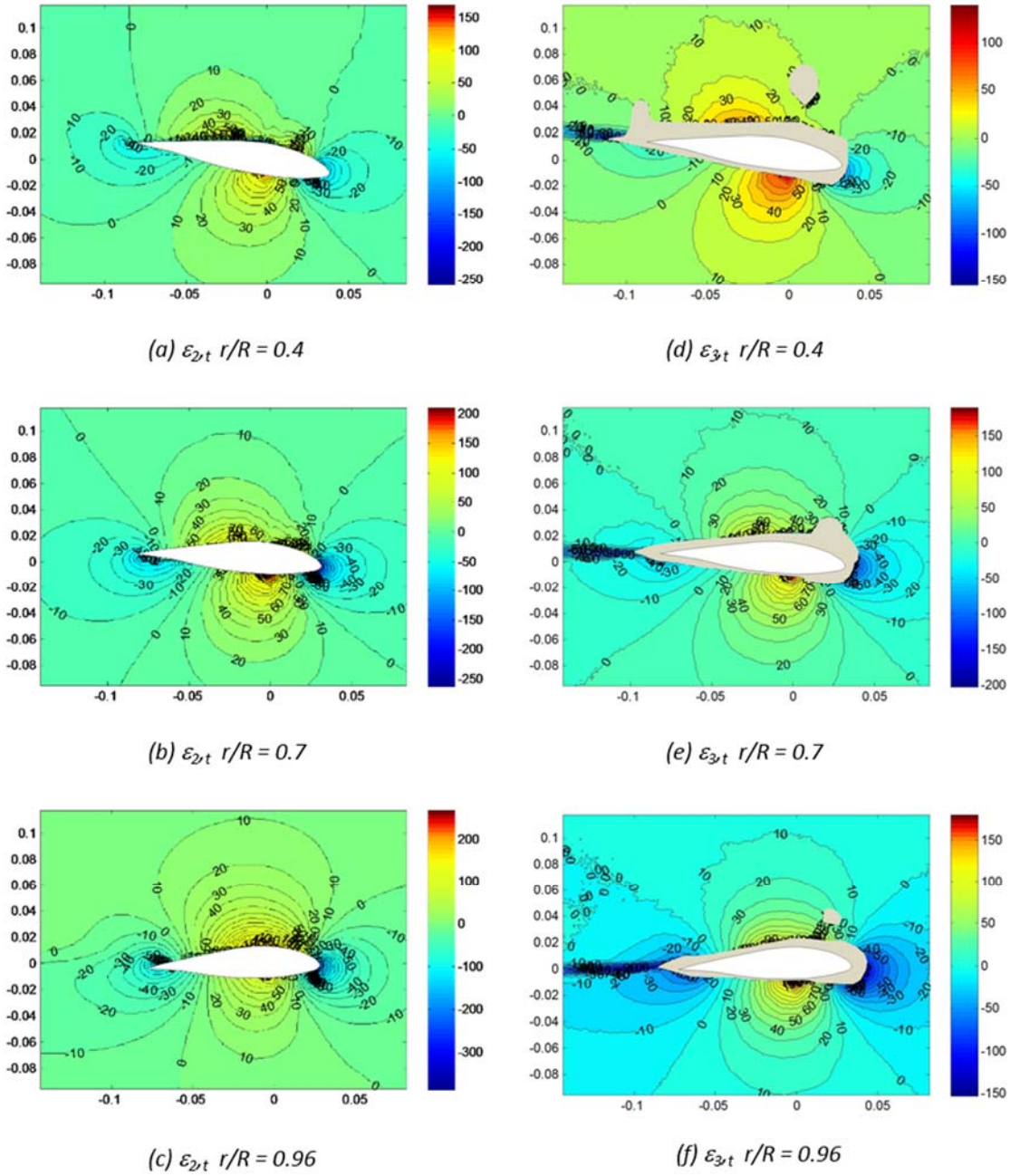

Figure 6: *Contour plots showing distributions for percentage errors $\varepsilon_{2,t}$((a)-(c)) and $\varepsilon_{3,t}$((d)-(f)) around the blades. The x and y coordinates for the flow domains are shown in metres.*

The level of agreement between $\varepsilon_{2,t}$ and $\varepsilon_{3,t}$ presented in Figures 6(a)-(c) and 6(d)-(e), respectively, is also reasonable good. Comparing Figures 5 and 6, it can be easily noted that the confined regions around the blades at which the errors predictions for the tangential flow are small do not coincide with those for axial flow. As opposed to axial flow, the confined regions of low $\varepsilon_{2,t}$ and $\varepsilon_{3,t}$ at the upper and lower blade surfaces tend to be located close to the leading and trailing edges rather than in the proximity of the mid-chord.

Figures 5(d)-(f) and 6(d)-(f) indicate masked regions surrounding the airfoil, which resulted from inaccuracies in the PIV measurements originating from the reflectivity of the blade surfaces. These regions were excluded, from the statistical analysis on the error results presented in this paper.

A statistical analysis was undertaken to estimate the total number of grid points n_a (and n_t) at which the errors $\varepsilon_{1,a}$, $\varepsilon_{2,a}$and $\varepsilon_{3,a}$ (and $\varepsilon_{1,t}$, $\varepsilon_{2,t}$ and $\varepsilon_{3,t}$) was less than different maximum error values. The analysis was repeated for each of the six radial locations (*r/R*) along the rotor blades. Given that *N* is the total number of data points within the domain, the cumulative error distribution for the probability of occurrence n_a/N (and n_t/N) could be derived from the error datasets computed using equations from Table 2.

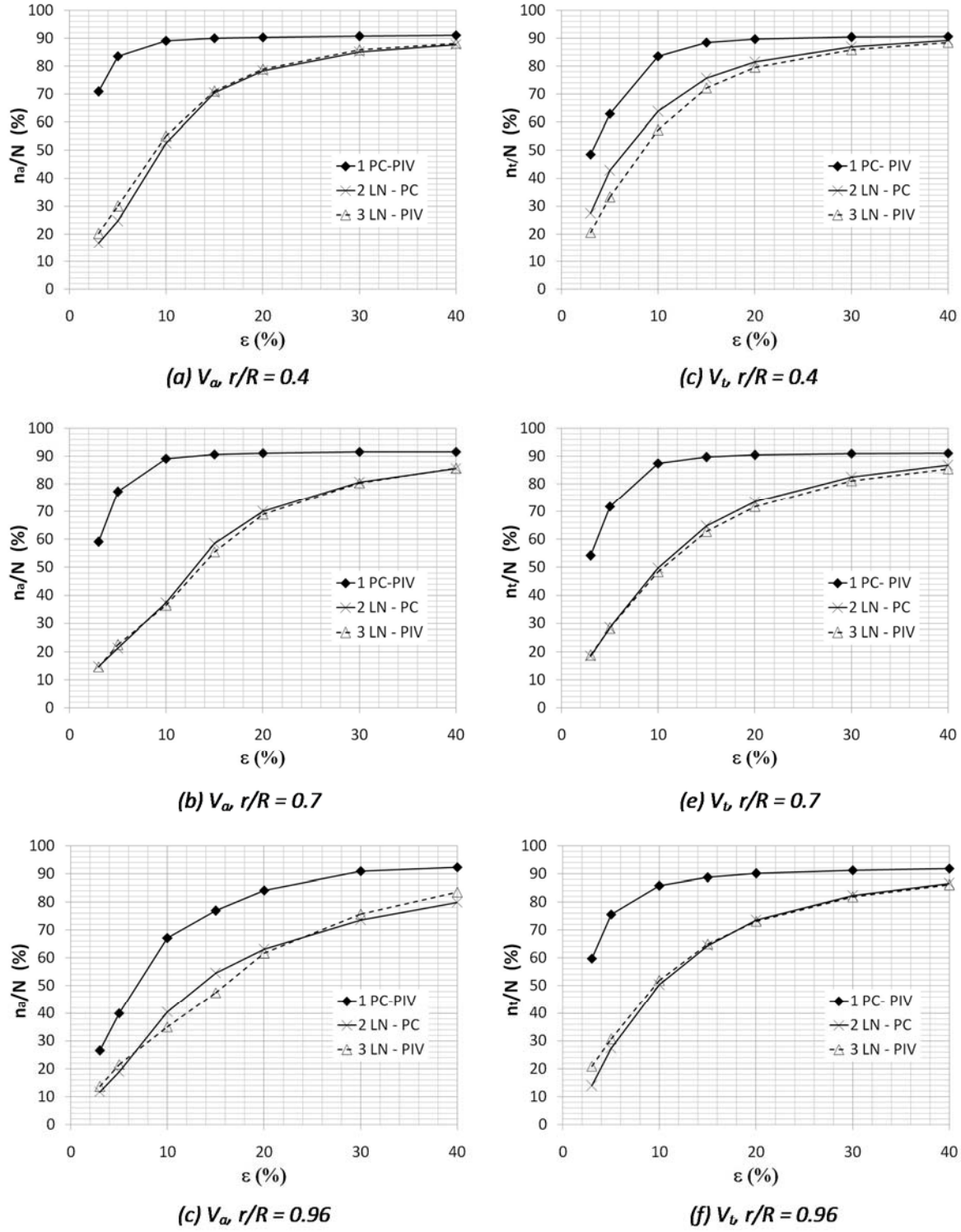

Figure 7: *Cumulative probability distributions for the errors in the predicted axial ((a)-(c)) and tangential ((d)-(f)) velocities around blades. ε_1 - 1 PC-PIV; ε_2 - 2 LN-PC; ε_3 - 3 LN-PIV. Δ=0.01m*

The cumulative error distributions for the axial velocity V_a at *r/R* equal to 0.4, 0.7 and 0.96 are shown in Figures 7(a)-(c) while those for the tangential velocity V_t are shown in Figures 7 (d)-(e). It may be observed that the probability of occurrences (n_a/N and n_t/N) for ε_1 which represents the error of the panel code predictions with respect to the PIV measurements, is significantly higher than those for ε_2 and ε_3. This quantitatively explains the limitations of the lifting-line free-wake model (LN) in simulating the flow characteristics in the close proximity of the wind turbine blades. The values of n_a/N and n_t/N may actually be assumed to be approximately equal to the area out the domain within which the error is below a given maximum allowable error. It may be observed from Figure 7 that, in the case of the lifting-line model predictions, this area only accounts to around 25-30% of the entire domain at a maximum allowable error of 5%. This is far lower than that for the panel vortex model predictions which lies in the range of 45-85%, depending on radial location. It should be pointed out that the n_a/N and n_t/N values for panel code predictions with respect to the PIV measurements do not reach the 100% limit for $\varepsilon_{1,a}$ and $\varepsilon_{1,t}$ <40%. This is due to errors associated with both the panel code and the PIV measurements.

The variations of the probabilities of occurrence in the prediction errors with radial location are presented in Figure 8. Only the probabilities for an allowable error limit of 5% are shown. Figure 8(a) shows the probabilities for the axial velocities while Figure 8(b) is related to the tangential velocity predictions. The n_a/N value for the panel code (PC) decreases appreciably at the blade tip, indicating increased error predictions when modelling the flow around the blades in the outer radial locations. In the case of the tangential velocities (Figure 8(b)), a different trend is observed, with the panel code (PC) n_t/N values increasing towards the tip of the blade but decreasing at the inboard location at *r/R* = 0.4. The probabilities of occurrences within the flow domain for the two independent lifting line model predictions (LN-PC and LN-PIV), are less sensitive to radial location. Yet these are still significantly lower than those for the panel code (PC-PIV). The n_a/N and n_t/N values for the lifting line predictions only decrease marginally at the outer blade sections. From a direct comparison of Figure 8(a) and 8(b), it can be noted that the values of n_t/N for the lifting line model (LN) errors $\varepsilon_{2,t}$and $\varepsilon_{3,t}$are slightly larger than the corresponding n_a/N values. This is being observed for the two independent lifting-line model predictions (LN-PC and LN-PIV). It can thus be concluded that the lifting line model is somewhat more reliable, tough only marginally, in predicting of tangential flow field than the axial flow one.

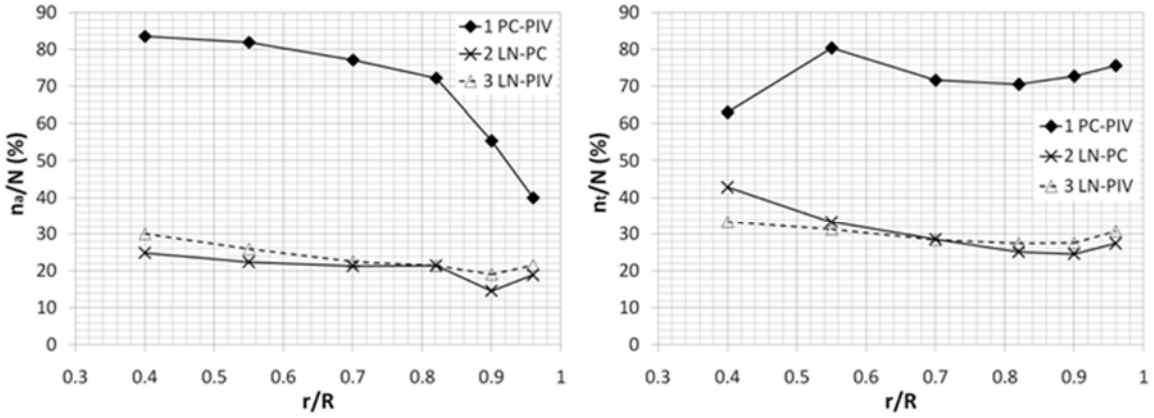

(a) *(b)*

Figure 8: *Variations for the error probabilities for the predicted axial (a) and tangential (b) flow velocity distributions around blades with radial location (r/R) for a maximum error (ε) of 5%.*
Δ=0.01m. ε_1 - 1 PC-PIV; ε_2 - 2 LN-PC; ε_3 - 3 LN-PIV

Further analysis in the present study involved the computation of the mean ε_m and standard deviation ε_{sd} of the estimated errors ($\varepsilon_{1,a}, \varepsilon_{2,a}, \varepsilon_{3,a}, \varepsilon_{1,t}, \varepsilon_{2,t}$ and $\varepsilon_{3,t}$) over a selected region within the flow domain. The region consisted of two rectangular areas, one located upstream and the other downstream of the blade section (refer to Figure 9). Distances (t_1,t_2) from the *x*-axis were taken as (0.04,0.08) metres. The mean and standard deviation of each error was computed using the following equations:

$$\varepsilon_m = \frac{1}{N}\sum_{i=0}^{N-1}|\varepsilon_i| \qquad (3a)$$

$$\varepsilon_{sd} = \frac{1}{N}\sum_{i=0}^{N-1}(|\varepsilon_i| - \varepsilon_m)^2 \qquad (3b)$$

The mean and standard deviation for lifting-line model errors $\varepsilon_{2,a}$and $\varepsilon_{3,a}$increase gradually with *r/R* for the outermost region (refer to

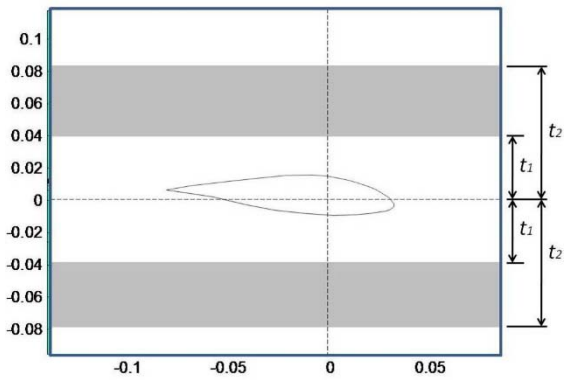

Figure 9: *Regions (shaded) with flow domain around blades across which $\varepsilon_m$and ε_{sd} were computed.*

Figures 10(a) and (b)). However a decrease may occur at the blade tip, as may be seen from Figure 10(a). Similar trends were noted for the mean and standard deviation values of the lifting-line model errors $\varepsilon_{2,t}$ and $\varepsilon_{3,t}$. Both ε_m and ε_{sd} for the lifting-line model remain considerably higher than those of the panel code.

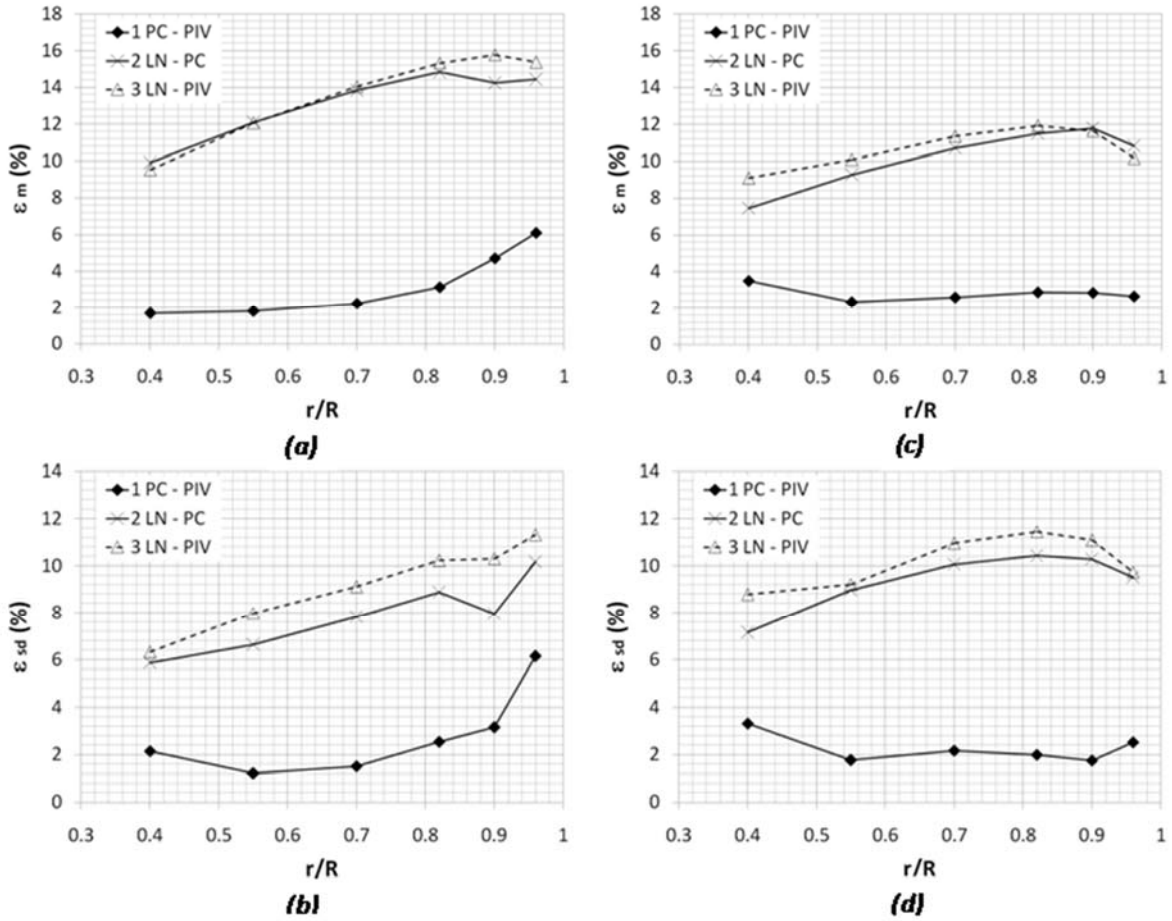

Figure 10: *Variations of the mean (ε_m) and standard deviation (ε_{sd}) of the errors in the predicted axial ((a)-(b)) and tangential ((c)-(d)) flow velocities with radial location (r/R) for region defined by (t_1, t_2) = (0.04, 0.08). Δ=0.01m. ε_1 - 1 PC-PIV; ε_2 - 2 LN-PC; ε_3 - 3 LN-PIV.*

8. Conclusions

This study has confirmed that the level of uncertainity in the axial and tangential flow field predictions from a lifting-line free wake model around a rotating wind turbine blade is significant. The assessment was based on two independent sources: numerical predications from a 3D panel method and PIV measurements. The analysis involved a statistical analysis at various radial location of the blade. The level of uncertaininty in the lifting line model estimates was found to vary considerably in the radial location. However there still exist confined areas in the flow domain close to a wind turbine blade at which the lifting line method can still predict both the axial and tangential flow velocities with a reliable degree of accuracy. Such confined areas for the axial flow velocity do not co-incide with those for the tangential flow fields. The study has also shown that the accuracy with which the lifting line method predicts the tangential component was found to be marginally higher that for the axial component.

References

[1]. Snel H., "Review of Aerodynamics of Wind Turbines", *Wind Energy*, Vol. 6, 2003, pp. 203-211.

[2]. Vermeer L.J, S∅rensen, J. N., and Crespo, A. "Wind turbine wake aerodynamics", *Progress in Aerospace Sciences*, 98:467-510.

[3]. Hansen, M., S∅rensen, J., Voutsinas, S., S∅rensen, N., and Madsen, H. (2006).State of the art in wind turbine aerodynamics and aeroelasticity. *Progress in Aerospace Sciences*, 42 Issue 4:285-330.

[4]. Sanderse, B. "Aerodynamics of wind turbine wakes", National Energy Research Foundation, ECN-E-09-016, 2009.

[5].Leishman J. G., Bhagwat M.J., and Bagai, A., "Free-Vortex Filament Methods for the Analysis of Helicopter Rotor Wakes", *Journal of Aircraft,* Vol. 39, No. 5, pp 759-775, 2002.

[6]. van Garrel, A., "Development of a Wind Turbine Aerodynamics Simulation Module", National Energy Research Foundation, ECN-C-03-079, 2003.

[7]. Voutsinas, S. G., Belessis, M. A. and Huberson, S., "Dynamic Inflow Effects and Vortex Particle Methods", Proceedings fr om the European Wind Energy Conferen ce, Lûbeck-Travemûnde, Germany, 1993.

[8]. Lee D. J. and Na, S. U., "Numerical Simulations of Wake Stru ctures Generated by Rotating Blades using a Time Marching Free Vortex Blob Method", *European Journal of Mechanics – B/Fluids, 1999.*

[9]. Del Campo, V., Ragni, D., Micallef, D., Akay, B., Diez, F. J., Simão Ferreira, C., "3D load calculation on a horizontal axis wind turbine using PIV", *Wind Energy,* August 2013.

[10]. D. Micallef. 3D flows near a HAWT rotor: A dissection of blade and wake contributions. PhD Thesis. TU Delft and University of Malta.

[11]. Ramasamy, M. and Leishman, J. G., "A Generalized Model for Transitional Blade Tip Vortices", *Journal of the American Helicopter Society*, 51(1):92-103, 2006.

[12]. Ramasamy, M. and Leishman, J. G., "A Reynolds Number-based Blade Tip Vortex Model". *Journal of the American Helicopter Society*, 52(3):214-223, 2007

[13]. Katz, J., Plotkin, A. Low-speed aerodynamics. *Cambridge University Press, Cambridge 2001.*

[14]. Simao Ferreira, C.J. The near wake of the VAWT: 2D and 3D views of the VAWT aerodynamics. *PhD Thesis, Technische Universiteit Delft, The Netherlands 2009.*

[15]. Micallef, D., van Bussel, G.J.W., Ferreira, C.S., Sant, T., "An investigation of radial velocities for a HAWT in axial and yawed flow", *Wind Energy*, Vol. 9, No. 6, pp. 549-577, 2006.

[16]. Sant T., van Kuik G.A.M. and van Bussel G.J.W., "Estimating the Angle of Attack from Blade Pressure Measurements on the NREL Phase VI Rotor using a Free-Wake Vortex Model: Axial Conditions", *Wind Energy*, Vol. 9, No. 6, pp. 549-577, 2006.